Multivariate singular spectrum analysis and the road to phase synchronization

Andreas Groth and Michael Ghil

Multivariate singular spectrum analysis and the road to phase synchronization

Andreas Groth[1, 2, *] and Michael Ghil[1, 2, 3]

[1] *Geosciences Department, Ecole Normale Supérieure, Paris, France*
[2] *Environmental Research & Teaching Institute, Ecole Normale Supérieure, Paris, France*
[3] *Department of Atmospheric & Oceanic Sciences and Institute of Geophysics*
& Planetary Physics, University of California, Los Angeles, USA

We show that multivariate singular spectrum analysis (M-SSA) greatly helps study phase synchronization in a large system of coupled oscillators and in the presence of high observational noise levels. With no need for detailed knowledge of individual subsystems nor any a priori phase definition for each of them, we demonstrate that M-SSA can automatically identify multiple oscillatory modes and detect whether these modes are shared by clusters of phase-and-frequency locked oscillators. As an essential modification of M-SSA, we introduce here variance-maximization (varimax) rotation of the M-SSA eigenvectors to optimally identify synchronized-oscillator clustering.

I. INTRODUCTION

Over the last two decades, singular spectrum analysis (SSA) and multivariate SSA (M-SSA) have proven their usefulness in the temporal and spatio-temporal analysis of short and noisy time series in several fields of the geosciences and of other disciplines [1]. M-SSA provides insight into the unknown or partially known dynamics of the underlying system by decomposing the delay-coordinate phase space of a given multivariate time series into a set of data-adaptive orthonormal components. These components can be classified essentially into trends, oscillatory patterns and noise, and allow one to reconstruct a robust "skeleton" of the dynamical system's structure [1–3]. While this skeleton does not yield, in general, the dimension of the system's attractor [2, 4, 5], we show here that it can greatly help phase synchronization analysis and provide considerable insight into the mechanisms of rhythm adjustment.

Phase synchronization refers, in general, to an adjustment of rhythms of coupled oscillators that is reflected in a locking of both their frequencies and phases [6, 7]. While for periodic orbits the phase is well defined, several methods exist to define a phase for more complex, possibly chaotic behavior. In the presence of spiral behavior, the phase is typically defined as an angle of rotation with respect to an origin in phase space [8–10]. In practice, however, this approach requires a priori information about the analyzed system, e.g. by visual inspection. It thus may become difficult to formulate a definition that is both useful and robust for a high-dimensional system and in the presence of noise.

In the present paper, we show that M-SSA is able to automatically identify oscillatory modes and detect cluster synchronization in large systems of coupled oscillators. We show that the M-SSA approach, which requires no detailed knowledge of individual subsystems nor a

suitable phase definition for each of them, provides an attractive alternative to commonly used phase-based approaches [8–10].

Feliks et al. [11] have suggested the application of M-SSA to pairs of climatic variables in order to determine mutual influence and synchronization between these variables. We introduce here, as a crucial modification of their idea, the rotation of M-SSA eigenvectors and provide numerical evidence for its improved ability to identify clusters of synchronized oscillators. This modification of classical M-SSA becomes more and more important as the number of coupled oscillators increases; results are given for a chain of coupled chaotic oscillators studied in [12]. Furthermore, we show that M-SSA provides insight into the reconstruction of shared dynamical behavior in terms of common oscillatory modes.

The paper is organized as follows. In Sec. II, we briefly review M-SSA and illustrate its properties on a prototypical model system. Furthermore, we present the novel idea of applying variance-maximization (varimax) rotation to M-SSA eigenvectors and the improvements in the analysis of clustering effects thus obtained. In Sec. III, we show how M-SSA can help phase synchronization analysis in a chain of coupled chaotic oscillators. The results are summarized and discussed in Sec. IV.

II. METHODS

A. Multivariate singular spectrum analysis

SSA and M-SSA rely on the classical Karhunen-Loève spectral decomposition of time series. Broomhead and King [13, 14] introduced them into dynamical systems analysis, as a more robust version of the Mañé-Takens idea to reconstruct dynamics from a single time series. We focus here on M-SSA, which we summarize for completeness.

Let $\mathbf{x} = \{x_d(n) : d = 1, \ldots, D, n = 1, \ldots, N\}$ be a multivariate time series with D channels of length N.

* Electronic address: andreas.groth@ens.fr

We assume that each channel has been centered and normalized. Following the original embedding ideas of Mañé and Takens, the starting point of M-SSA is to embed each channel into an M-dimensional phase space, by using lagged copies $\mathbf{X}_d(n) = (x_d(n), \ldots, x_d(n + M - 1))$, $n = 1, \ldots, N - M + 1$. From this we form the full augmented trajectory matrix $\mathbf{X} = (\mathbf{X}_1, \mathbf{X}_2, \ldots, \mathbf{X}_D)$, which has DM columns of length $N - M + 1$.

The M-SSA algorithm then computes the covariance matrix $\mathbf{C} = \mathbf{X}^\mathsf{T}\mathbf{X}/N$ of $\mathbf{X}$ and its eigendecomposition; here $(\cdot)^\mathsf{T}$ indicates transposition. The covariance matrix $\mathbf{C}$ combines all auto- as well as cross-covariances, up to a time lag equal to $M - 1$. Due to finite-size effects, the sample $\mathbf{C}$ may deviate slightly from symmetry and be biased, but effective and accurate estimation methods appear in Ref. [1].

Next, one diagonalizes the appropriately symmetrized covariance matrix

$$\mathbf{\Lambda} = \mathbf{E}^\mathsf{T}\mathbf{C}\,\mathbf{E} \qquad (1)$$

to yield a diagonal matrix $\mathbf{\Lambda}$ that contains the real eigenvalues λ_k of $\mathbf{C}$, and a matrix $\mathbf{E}$ whose columns are the associated eigenvectors $\mathbf{e}_k$. The $\mathbf{e}_k$'s form a new orthogonal basis in the embedding space of $\mathbf{X}$, and the corresponding λ_k's give the variance in the direction of $\mathbf{e}_k$. The spectral decomposition in Eq. (1) determines the directions of greatest variance successively, from largest to smallest, subject to the condition that each new direction be orthogonal to all the preceding ones.

Projecting the time series $\mathbf{X}$ onto the eigenvectors,

$$\mathbf{A} = \mathbf{X}\mathbf{E}, \qquad (2)$$

yields the corresponding *principal components (PCs)* as the columns of $\mathbf{A}$. The PCs have the same length $N - M + 1$ as $\mathbf{X}$ and are uncorrelated at zero lag; they can be considered as filtered components of the time series $\mathbf{x}$, with data-adaptive filters that are given by the eigenvectors [15]. This filtering property becomes more obvious if we rewrite Eq. (2) explicitly as

$$a_k(n) = \sum_{d=1}^{D}\sum_{m=1}^{M} x_d(n + m - 1)e_{dk}(m), \qquad (3)$$

with $k = 1, \ldots, DM$ and $n = 1, \ldots, N - M + 1$. In particular, setting $M = 1$ reduces M-SSA to classical principal component analysis (PCA) in D variables.

The coefficients $a_k(\cdot)$ are the entries of the PC matrix $\mathbf{A}$. The notation $\mathbf{e}_k = \{e_{dk}(m) : 1 \le d \le D\}$ is meant to reflect the special structure of the eigenvectors, which are composed of D consecutive segments of length M, each of which is associated with a channel, $e_{dk}(m) \equiv e_k(\{d - 1\}M + m)$. Hence, the summation over m in Eq. (3) can be interpreted as a classical finite-impulse response (FIR) filter [16] operating on channel d with filter coefficients given by the eigenvector elements $e_{dk}(m)$. The second summation over d, which combines the filtered channels, represents a classical PCA.

In contrast to PCA eigenvectors, M-SSA eigenvectors are, therefore, able to capture oscillatory behavior in time via *oscillatory pairs* [2, 17]. Provided the two eigenvectors of a pair correspond to the same period, they are the data-adaptive equivalent of sine-and-cosine pairs in Fourier analysis. It is especially this property that enables M-SSA, in contrast to PCA, to represent temporal oscillations, and hence makes M-SSA superior to PCA in phase synchronization analysis.

Several papers have explored recently the benefits of an eigenvalue decomposition in the context of synchronization analysis. Müller and coauthors used PCA eigenvalues to derive the synchronization strength of two coupled chaotic oscillators [18]. In [19], the authors presented a participation index in order to identify clusters of synchronized oscillators. Feliks and coauthors applied similar ideas to climatic oscillators [11].

M-SSA, however, goes beyond a pure identification and quantification of coupled behavior: it allows, furthermore, to reconstruct the dynamical behavior that the coupled subsystems share and that is associated with a specific eigenvalue-eigenvector pair. The PCs, which are already filtered versions of the original time series, are not appropriate for this purpose, since they combine the properties of all the channels in the data set. Moreover, the PCs have a reduced length $N - M + 1$ and do not allow a unique localization in time [1, 3].

A way to reconstruct the individual components of the system's behavior that is optimal in the least-squares sense is given by the transformation

$$r_{dk}(n) = \frac{1}{M_n}\sum_{m=L_n}^{U_n} a_k(n - m + 1)e_{dk}(m). \qquad (4)$$

The r_{dk} are referred to as *reconstructed components (RCs)* [15, 17] and represent that part of channel x_d that corresponds to the eigenelement pair $(\lambda_k, \mathbf{e}_k)$. The values of the normalization factor M_n and the summation bounds L_n and U_n for the central part of the time series, $M \le n \le N - M + 1$, are simply $(M_n, L_n, U_n) = (M, 1, M)$; for either end they are given in [1]. In particular, the time series can be completely reconstructed by the sum of all its RCs, $x_d(n) = \sum_{k=1}^{DM} r_{dk}(n)$. In the univariate case $D = 1$, Eqs. (3) and (4) specify forward-and-reverse filtering, respectively, and therefore the resulting RCs have zero-phase distortion [16].

B. Model equations

To illustrate the insights provided by M-SSA into phase synchronization, we consider a chain of diffusively coupled Rössler oscillators [12]:

$$\begin{aligned}
\dot{x}_j &= -\omega_j y_j - z_j, \\
\dot{y}_j &= \omega_j x_j + \alpha\,y_j + c\,(y_{j+1} - 2y_j + y_{j-1}), \qquad (5)\\
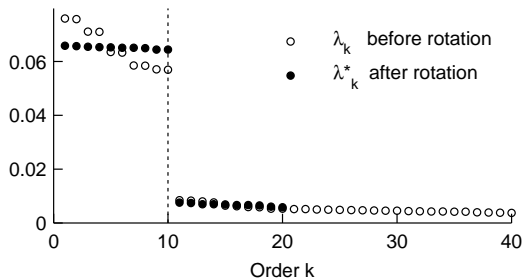\dot{z}_j &= 0.1 + z_j(x_j - 8.5).
\end{aligned}$$

Figure 1. Eigenvalue spectrum for five uncoupled and detuned Rössler oscillators, with $c = 0$ and $\alpha = 0.15$ in Eq. (5): λ_k from Eq. (1), and modified variances λ_k^* from Eq. (12) after rotation of the first $S = 20$ eigenvectors. The window width $M = 30$ covers more than one oscillation period, since $M\Delta t = 12$, while the mean period is roughly $2\pi/\omega_j \simeq 6$.

Figure 2. Eigenvectors $\mathbf{e}_k$ corresponding to the 10 largest eigenvalues λ_k in Fig. 1. Each eigenvector of length DM is composed of $D = 15$ consecutive segments, each of length $M = 30$, associated with the 15 channels.

The position in the chain is given by the index $j = 1, \ldots, J$; $\omega_j = \omega_1 + 0.02(j - 1)$ are the associated natural frequencies, with $\omega_1 = 1$, and we assume free boundary conditions: $x_0(n) = x_1(n)$, $x_{J+1}(n) = x_J(n)$. The frequency mismatch $\Delta_{jk}\omega$ between oscillators j and k is often called "detuning" in engineering applications; here $\Delta_{jk}\omega = 0.02|j - k|$. The parameter α allows one to change the system's topology [9] and $c > 0$ is the coupling strength.

We first set $\alpha = 0.15$ and the individual oscillators, while being chaotic, are in a phase-coherent regime, with a well-defined center of oscillation in the (x, y)-plane [8, 9]. We integrate $J = 5$ uncoupled system, with $c = 0$, in order to see whether M-SSA is able to distinguish between the different oscillators. The solution is sampled at time intervals $\Delta t = 0.4$, and the observed time series $\mathbf{x}$ has $D = 3J = 15$ channels of length $N = 2500$. To cover more than one oscillation period, we select a window width of $M = 30$, which yields $DM = 450$ eigenvalues and eigenvectors, respectively, by using Eq. (1). The 40 largest eigenvalues λ_k are plotted in Fig. 1 (open circles).

The leading 10 eigenvalues are clearly significant and fall into five pairs of nearly equal ones. The eigenvalue spectrum in Fig. 1 thus indicates that our M-SSA has correctly identified the five uncoupled oscillators in Eq. (5): each of them is described by an oscillatory pair, which shares its natural frequency (not shown).

An inspection of the corresponding eigenvectors in Fig. 2, however, shows a more ambiguous picture: The eigenvectors do not distinguish between the distinct, uncoupled systems. Instead the distinct systems are all present in each of the eigenvectors. Moreover, as the number J of coupled oscillators increases, the separation between the significant λ_k's and those that are not disappears (not shown), and so does the gap present in Fig. 1.

This mixture is a shortcoming of PCA in general and of M-SSA in particular. This type of methods is designed to capture a maximum of the variance in the data 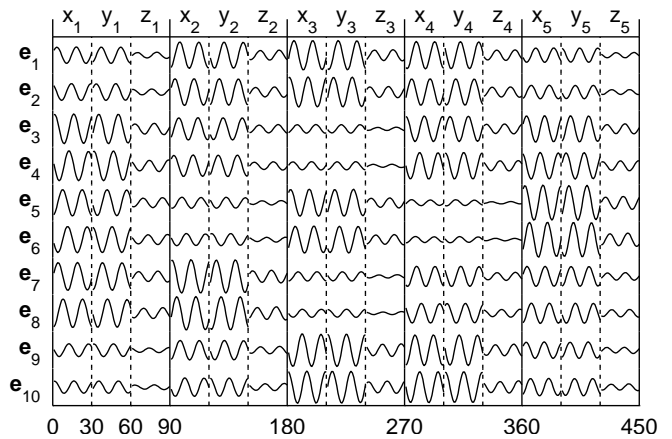set with a minimum number of PCs [1, 20]: while good for signal compression purposes, they contribute but little to the physical interpretation of the underlying dynamical system. In the example at hand, all five modes have the same variance, and thus signal compression does not necessarily reveal the correct underlying structure, only a mixture of degenerate eigenvectors [20].

C. Varimax rotation

As the number D of channels increases, so does the risk of degenerate eigenvectors in all types of PCA. This was less of a problem in [11], where $D = 2$. The participation index proposed in [19], however, suffers precisely from these mixing problems. Allefeld and coauthors [19] discussed therefore a heuristic approach of setting eigenvector coordinates to zero and rerunning the analysis. Despite this iterated analysis, correct identification of the underlying cluster structure is only partially possible, in particular when the clusters have similar strength [21].

Recently, Vejmelka and Paluš [22] found *varimax orthogonal rotation* [23] to be helpful in better identifying the correct cluster structure. In this paper, we rely on the same principles of eigenvector rotation, as widely used in PCA [24], but in the context of M-SSA. As we shall see, it is the special structure of M-SSA eigenvectors that requires an adaptation of the varimax algorithm.

First, we briefly review the classical methodology of varimax rotation. The idea that all so-called *simple-structure rotations* have in common is to find a posterior eigenvector rotation that simplifies the structure of the eigenvectors, reduces mixture effects and thus improves the physical interpretability. There are several ways to quantify the simplicity of a structure and to transform eigenvectors [25]. Varimax rotation attempts to do this by computing an appropriate orthogonal rotation $\mathbf{E}^* = \mathbf{E}\mathbf{T}$ to maximize the variance of the squared

elements of $\mathbf{E}^*$. This way, all the elements are brought close to either one or zero, while intermediate values that get in the way of a clear classification are eliminated.

In PCA with $M = 1$, as applied to factor analysis [23] or to random fields [25], varimax simply maximizes the variance of the squared elements e_{dk}^* of the eigenvectors $\mathbf{e}_k^*$ in $\mathbf{E}^*$,

$$V_1 = \sum_{k=1}^{S} \left\{ \frac{1}{D} \sum_{d=1}^{D} \left(\frac{e_{dk}^{*\,2}}{h_d^{*\,2}} \right)^2 - \left(\frac{1}{D} \sum_{d=1}^{D} \frac{e_{dk}^{*\,2}}{h_d^{*\,2}} \right)^2 \right\}, \quad (6)$$

where S is the number of rotated $\mathbf{e}_k^*$'s, and $h_d^{*\,2} = \sum_{k=1}^{S} e_{dk}^{*\,2}$ is the corresponding normalization. Kaiser [23] gives an explicit equation for the sequential rotation of pairs of $\mathbf{e}_k^*$ that shows this algorithm's simplicity of implementation and thus superiority over more sophisticated optimization procedures, such as independent component analysis.

In the criterion V_1, the variance is maximized over all the coordinates of the eigenvectors. As already discussed, M-SSA eigenvectors differ in structure from those of classical PCA and this difference impedes the direct application of varimax to the former: The rotation would not only achieve the desirable effect of increasing the difference between the FIR filters of length M, but also increase the variance within each of them; the latter effect is undesirable, since it can lead to a loss of correctly captured oscillatory pairs [17].

To avoid this loss of a key M-SSA property, we propose here a simple but effective modification of the varimax criterion. Prior to the calculation of the variance, we sum over the individual filters,

$$\bar{e}_{dk}^{*\,2} = \sum_{m=1}^{M} e_{dk}^{*\,2}(m), \quad (7)$$

and the criterion becomes

$$V_M = \sum_{k=1}^{S} \left\{ \frac{1}{D} \sum_{d=1}^{D} \left(\frac{\bar{e}_{dk}^{*\,2}}{\bar{h}_d^{*\,2}} \right)^2 - \left(\frac{1}{D} \sum_{d=1}^{D} \frac{\bar{e}_{dk}^{*\,2}}{\bar{h}_d^{*\,2}} \right)^2 \right\}, \quad (8)$$

with the normalization $\bar{h}_d^{*\,2} = \sum_{k=1}^{S} \bar{e}_{dk}^{*\,2}$. In this way, the criterion V_M attempts to bring the squared amplitudes of the filters either close to one or to zero; for $M = 1$ we recover the original criterion V_1.

With the modified criterion above, we have simply to replace — in the equation of pairwise rotation of two eigenvectors $\mathbf{e}_k$ and $\mathbf{e}_l$ in Ref. [23] — each $e_{dk}^2 + e_{dl}^2$ by its averaged version $\sum_m e_{dk}^2(m) + \sum_m e_{dl}^2(m)$, as well as each $e_{dk}e_{dl}$ by $\sum_m e_{dk}(m) \sum_m e_{dl}(m)$ (see Appendix A).

Typically, the rotation is restricted to the first S eigenvectors, which capture most of the systems' variance. In order to find an appropriate subset of eigenvectors, it is common to look for a gap in the eigenvalue spectrum; this approach is called a *scree test* [26], also referred to as a scree-diagram test [1]. An obvious gap as in Fig. 1, however, cannot be expected in general, especially in applications to short and noisy time series [1]. As mentioned
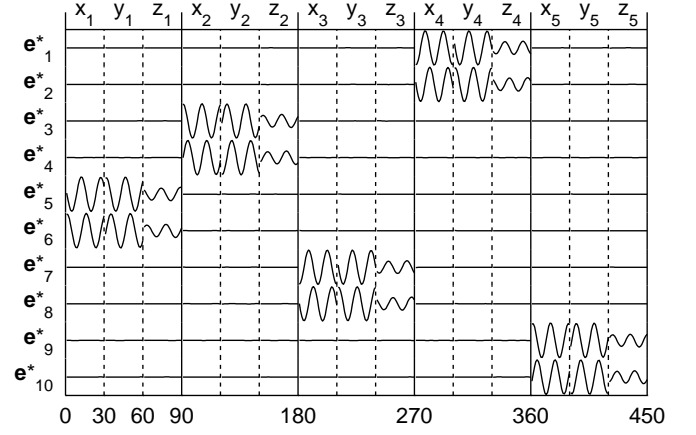

Figure 3. Rotated eigenvectors $\mathbf{e}_k^*$ after varimax rotation of the first $S = 20$ eigenvectors. Note that only the first 10 significant eigenvectors are shown.

already, this gap disappears as J, and hence D, increases. Therefore, numerous objective criteria for determining S have been proposed, but no general consensus exists; see for example [25] and references therein.

In our experience with real data, multiplying each eigenvector $\mathbf{e}_k$ by the singular value $\lambda_k^{1/2}$, prior to varimax, stabilizes the rotation results over a large range of S-values. Without this scaling, varimax would be susceptible to "overrotation" [27] and could end up with too many clusters for large S. Note that, for $M = 1$, the expression $\lambda_k e_{dk}^{*\,2}$ is the participation index of channel d in cluster k [19]; therefore, scaling the eigenvectors prior to varimax rotation maximizes the association into clusters and minimizes intermediate participation indices [22].

The scaling is only used to derive the rotation matrix $\mathbf{T}$: we multiply the S original leading eigenvectors, which form the columns of $\mathbf{E}_S$, by this $\mathbf{T}$, to yield

$$\mathbf{E}_S^* = \mathbf{E}_S \mathbf{T}. \quad (9)$$

There are two reasons for doing so: first, scaling, rotating and rescaling yields an oblique rotation, which does not perform as well as an orthogonal rotation in the present examples; second, the algorithm (9) preserves the variance captured by $\mathbf{E}_S$.

The result of eigenvector rotation is shown in Fig. 3. In contrast to the unrotated eigenvectors in Fig. 2, the rotated ones are clearly associated pairwise with each of the uncoupled oscillators and permit their unique identification. The rotated eigenvectors form oscillatory pairs that share the natural frequencies of the Rössler oscillators (not shown).

The number of rotated eigenvectors, in this case $S = 20$, has been chosen to include at least those that are significant. Even when rotating many more eigenvectors, $S = 40$ or 60 say, one obtains the same picture (not shown). This is a consequence of the eigenvector scaling prior to varimax, since adding more eigenvectors with small amplitude does not alter the variance V_M.

Next, in order to obtain the variance that the rotated eigenvectors capture, we project the covariance matrix $\mathbf{C}$ onto them,

$$\mathbf{\Lambda}_S^* = \mathbf{E}_S^{*\mathsf{T}} \mathbf{C} \, \mathbf{E}_S^*, \tag{10}$$

like in Eq. (1). Since the rotated eigenvectors $\mathbf{E}_S^*$ are not part of the singular value decomposition of the covariance matrix $\mathbf{C}$, the matrix $\mathbf{\Lambda}_S^*$ is not diagonal. From the equivalent formulation $\mathbf{\Lambda}_S^* = \mathbf{E}_S^{*\mathsf{T}} \mathbf{X}^\mathsf{T} \mathbf{X} \, \mathbf{E}_S^*/N = \mathbf{A}_S^{*\mathsf{T}} \mathbf{A}_S^*/N$ we see, however, that $\mathbf{\Lambda}_S^*$ does capture the variance of the *rotated PCs*,

$$\mathbf{A}_S^* = \mathbf{X} \, \mathbf{E}_S^* \equiv \mathbf{A}_S \, \mathbf{T}, \tag{11}$$

along its diagonal; we denote its diagonal elements by λ_k^* and call them the *modified variances*.

Figure 1 shows the resulting λ_k^*'s (solid circles) along with the original eigenvalues λ_k (open circles). Since M-SSA, like all PCA methods, tries to maximize variance captured by successive eigenvectors, it is also prone to artificial variance compression, i.e. it may account for too much variance in the largest eigenvalues or too little in the smallest. This flaw is reflected in the 10 largest λ_k's in Fig. 1 being unequal, although the oscillators have the same variance.

It is this variance compression that causes the gap between the original λ_k's to disappear as D increases. The values of the post-rotation λ_k^*'s, on the other hand, are now correctly associated with the individual oscillators, and do reflect the correct situation of equal variance. Note that the a priori choice of S is not critical with respect to the results in Fig. 1: even when rotating many more eigenvectors, one obtains the same distribution of λ_k^*'s (not shown).

As already stated above, an orthogonal rotation preserves the total variance captured by the λ_k^*'s. Inserting Eq. (9) into Eq. (10) yields the relationship

$$\mathbf{\Lambda}_S^* = \mathbf{T}^\mathsf{T} \mathbf{\Lambda}_S \mathbf{T}, \tag{12}$$

which is a similarity transformation and thus preserves the trace, i.e., the sum of the variances, during rotation.

Equation (4) was used first to derive the original RCs and is now applied directly to the rotated eigenvectors $\mathbf{E}_S^*$ and the PCs $\mathbf{A}_S^*$; the resulting RCs are denoted by r_{dk}^*. Since the rotation is based on successive planar rotations, the first S rotated eigenvectors and the remaining unrotated ones are still orthogonal, and the RCs r_{dk}^* thus add up to the original time series. In contrast to the unrotated RCs, we observe that the rotated RCs allow a good reproduction of oscillatory behavior (Fig. 4(a)).

D. Participation index

By analogy with the participation index $\lambda_k \, e_{dk}^{*2}$ in [19], we introduce here a *participation index*

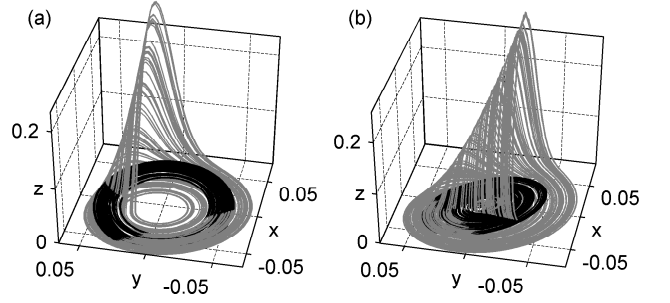$$\pi_{dk} = \lambda_k^* \, \bar{e}_{dk}^{*2} \tag{13}$$

Figure 4. Reconstruction of the leading pair, i. e. RCs 1-2 (black curve), of the coupled Rössler oscillators' actual trajectory (gray curve) in (a) a phase-coherent regime with $\alpha = 0.15$; and (b) in the funnel regime with $\alpha = 0.28$.

for M-SSA by replacing e_{dk}^{*2} with $\bar{e}_{dk}^{*2}$ from Eq. (7). Since the eigenvectors have norm one, $\sum_{d=1}^D \pi_{dk} = \lambda_k^*$. Consequently, π_{dk} quantifies the contribution of channel d to the variance λ_k^* of the k-th principal component.

III. PHASE SYNCHRONIZATION RESULTS

A. Phase-coherent oscillators

So far, we discussed the case of uncoupled oscillators and showed the ability of M-SSA to correctly identify the distinct oscillatory modes. We present next its ability to provide considerable insight into the mechanisms of rhythm adjustment on the road to phase synchronization.

We consider a chain of $J = 10$ Rössler oscillators (5) and take time series of length $N = 25\,000$. When the frequency mismatch in the model equations is sufficiently large, it is known that the transition in the observed mismatch is no longer smooth as the coupling strength c increases, and it occurs in abrupt jumps instead [12].

In the present case, $\Delta_{j,j+1}\omega = 0.02$ with $1 \leq j < j + 1 \leq J = 10$, synchronization manifests itself via clustering: the oscillators form clusters with the same observed frequency and even larger detuning between clusters. As c increases further, the number of clusters decreases in a cascade of vanishing frequencies; see Fig. 5(a).

We concentrate first on the identification of oscillatory modes and on their relation to clusters of phase-and-frequency locked oscillators. Note that the successive clustering of oscillators is also reflected in a decreasing number of significant eigenvalues λ_k in Fig. 5(b). The explanatory power of M-SSA, though, is quite limited in the absence of rotation. For weak coupling ($c \lesssim 0.018$), prior to any clustering, the spread among the largest λ_k's increases with c. This spread results from the already mentioned tendency to variance compression. As clustering sets in at $c \simeq 0.018$, the behavior at the successive bifurcation points is fairly smooth, with continuously decreasing eigenvalues and no distinct transitions. Further-
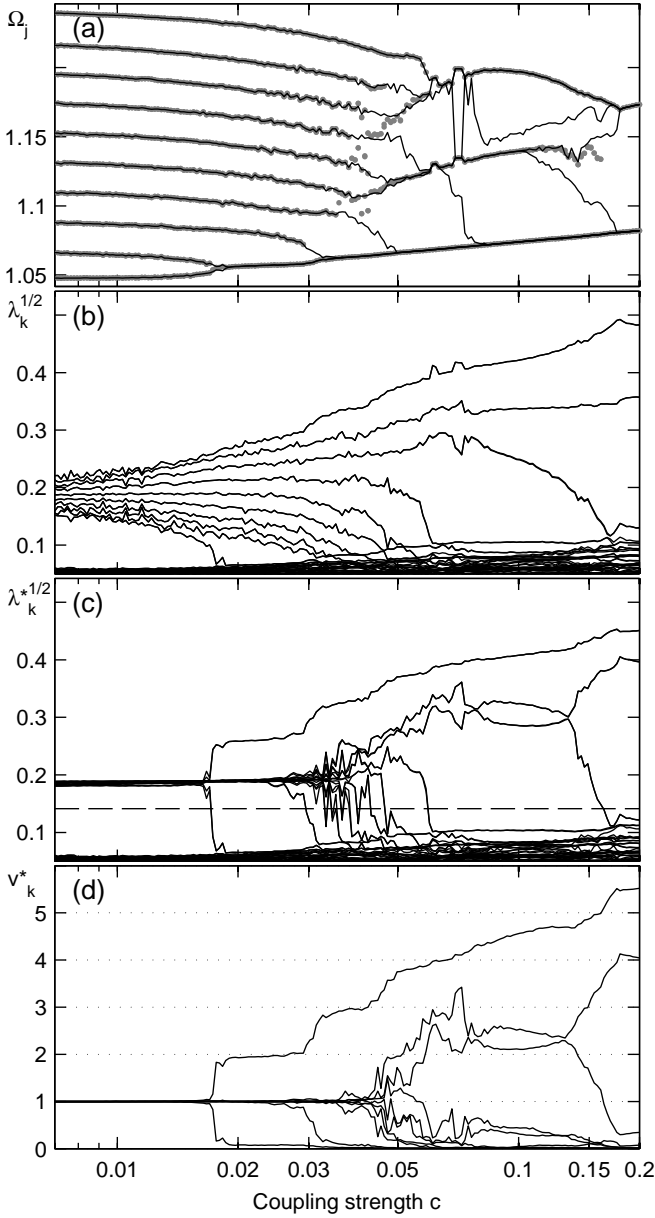
Figure 5. Synchronization for a chain of $J = 10$ coupled Rössler oscillators. (a) Mean observed frequencies $\Omega_j = \langle \dot{\phi}_j \rangle$, $\phi_j = \arctan(y_j/x_j)$, of the oscillators (solid lines) and estimated frequencies from rotated PCs (gray dots); (b) eigenvalue spectrum λ_k of M-SSA with $M = 30$; (c) modified variances λ_k^* after rotation of the first $S = 20$ eigenvectors, along with the remaining unchanged eigenvalues λ_k, $k \geq 21$; and (d) modified eigenvalues v_k^* of the matrix of pairwise phase coupling indices. Note logarithmic scale on x-axis.

more, no obvious gap that would allow a clear separation of significant eigenvalues appears, at $c \simeq 0.05$.

After rotation, however, the distribution of the λ_k^*'s in Fig. 5(c) reflects much better the transition to phase synchronization, with sharp jumps at the bifurcation points. The effect of variance compression has practically disappeared and we are able to clearly identify the signifi-

cant λ_k^*'s. Each line in the spectrum of the λ_k^*'s is now the superposition of two practically identical values — referred to as an oscillatory pair — and represents one oscillatory mode. These oscillatory modes, in turn, can be associated with the individual clusters of phase-and-frequency locked oscillators. At each bifurcation point, when the cluster structure changes and a frequency vanishes in Fig. 5(a), we observe an abrupt jump in Fig. 5(c).

An oscillatory mode's frequency, which one can estimate from the corresponding eigenvectors or PCs, matches very well the observed frequency in Fig. 5(a). In this figure, we have included only pairs with λ_k^*-values that lie above a certain threshold (dashed line in Fig. 5(c)), but in practice more sophisticated significance tests may be necessary [28]. There are only a few lines in Fig. 5(c) that are not covered by M-SSA. We will address this apparent mismatch when discussing the reconstruction of dynamical behavior later on.

We compare now the M-SSA results with the recently proposed clustering algorithm of [22], which relies on the matrix $\mathbf{P} = (\rho_{kl})$ of pairwise phase coupling indices $\rho_{kl} = |\langle \exp\{i(\phi_k - \phi_l)\}\rangle|$. The eigendecomposition of this matrix yields non-vanishing eigenvalues and associated eigenvectors that allow an accurate cluster identification, with a cluster's strength equal to the corresponding eigenvalue [22].

We propose here again, in contrast to [22], to scale the eigenvectors of $\mathbf{P}$ prior to variance maximization, as done for M-SSA in Sec. II C. The phase-coupling matrix $\mathbf{P}$ is symmetric but, unlike the covariance matrix $\mathbf{C}$, it is not necessarily positive semi-definite. Hence we set any negative eigenvalues to zero and obtain a rotation matrix for all D eigenvectors, which also helps us derive modified eigenvalues v_k^*, as in Eq. (12).

The results in Fig. 5(d) agree quite well with the M-SSA results in Fig. 5(c). For weak coupling, $c \lesssim 0.03$, the oscillators are uniquely associated into clusters, and the v_k^*'s are integers. For intermediate coupling, $0.03 \lesssim c \lesssim 0.2$, the number of clusters decreases, while connections between clusters (cluster-to-cluster) come into play and impede a unique cluster assignment; hence the resulting v_k^*-values are no longer integers.

We analyze next, in greater detail, the underlying cluster structure of locked modes. In order to understand the dynamical behavior of cluster-to-cluster interactions, we determine the associated RCs just before the transition from three to two clusters, at $c \simeq 0.12$ (Fig. 6). M-SSA detects three clusters, which comprise oscillators 1–4, 6-7, and 9-10, respectively. At the boundaries between two clusters, we see that the oscillators $j = 5$ and $j = 8$ are not uniquely classified, since they possess non-vanishing RCs in both clusters.

The power spectra of uniquely classified oscillators, e.g. of their x-components (not shown), are characterized by a strong single peak at the observed frequency Ω. At the boundaries between two clusters, the behavior of the oscillators is fairly intermittent and the trajectories exhibit beats, while their power spectra possess two peaks,
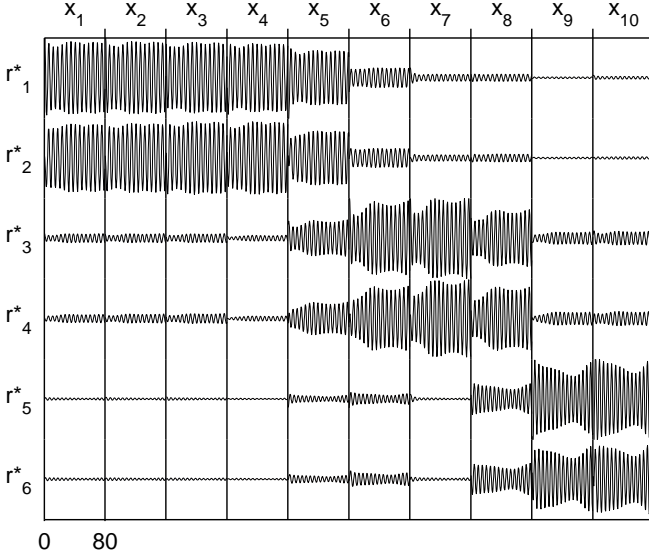
Figure 6. Reconstructed components RCs 1–6 of the system shown in Fig. 5(c) at coupling strength $c = 0.12$. Note that only a part of the x–components is shown.
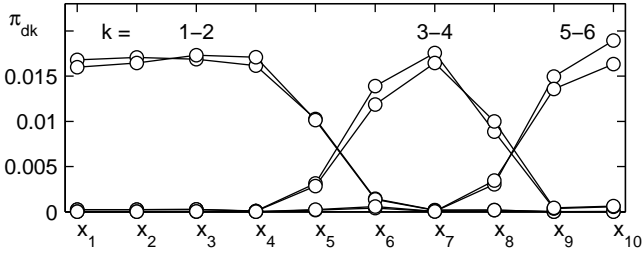

Figure 7. Participation index π_{dk} that correspond to Fig. 6. The values for the clusters $k = (1, 2)$, $(3,4)$ and $(5,6)$ are clearly well separated, while intermediate values are assigned to oscillators $j = 5$ and 8.

at the frequencies of the two clusters, respectively. With increasing coupling strength, energy is transferred from one peak to the other, and M-SSA shows a rather abrupt vanishing of one of the oscillatory pairs, as soon as the middle cluster has vanished (Fig. 5(c)). This transfer of energy is reflected by a smooth change in the observed frequencies Ω_j in Fig. 5(a), which correspond to an average frequency for each oscillator.

If solely interested in the cluster structure, and not in the detailed dynamical behavior, we can obtain this structure directly by means of the participation index π_{dk}. Without the need for an explicit calculation of the PCs and RCs, π_{dk} quantifies the contribution of channel d to the variance λ_k^* of the kth PC. In agreement with the RC findings of Fig. 6, intermediate π–values are assigned to the oscillators $j = 5$ and $j = 8$ at the cluster boundaries, while the π–values for the other oscillators j are close to either 0 or the unique value associated with a given cluster; see Fig. 7.

Next, we wish to evaluate the robustness of the clus-

tering analysis in the presence of observational noise, and add Gaussian white noise with the same variance as the signal. In spite of this very high noise level, the M-SSA results are visually the same (Figs. 8(a),(c)), because the noise variance in each principal direction is reduced by a factor DM and large eigenvalues remain, therefore, virtually unaffected. Even when the noise starts swamping the signal, as is the case here, the RCs in Fig. 4 and Fig. 6 remain visually the same (not shown) and provide a robust reconstruction of oscillatory behavior. Synchronization analysis methods, however, that use a geometric phase definition are affected much more strongly by the presence of noise, and can no longer provide correct cluster identification (Figs. 8(b),(d)).

Moreover, PCA eigenvalues and PCs are invariant with respect to an arbitrary orthogonal rotation of the time series $\mathbf{x} = \{x_d(n)\}$, a theoretical result confirmed by numerical tests on the invariance of M-SSA eigenvalues and PCs; hence rotation does not alter the M-SSA results in Figs. 5(a–c). The proper definition of a phase — such as the one used in Fig. 5(d) — does depend, however, on the coordinate-wise representation of the dynamical system and is thus not invariant with respect to rotation.

B. Funnel regime with no phase coherence

In the previous section we have considered the phase-coherent regime of Rössler oscillators that share a rather simple spiral topology. The power spectrum of each oscillator contains, in this case, a well-pronounced peak and synchronization manifests itself mainly in a locking of both phase and frequency. As a result, M-SSA can easily detect clusters of synchronized oscillators in terms of oscillatory pairs.

We expect, however, to be confronted in many realistic cases with oscillatory behavior on different time scales and with dynamics that gives rise to a more complicated topology. The so-called *funnel regime* of the Rössler system (5) is a well-studied, paradigmatic example of such a situation [9]. In this regime, the attractor has lost its spiral topology and a straightforward phase definition becomes difficult (Fig. 4(b)).

The dynamics is no longer phase-coherent and the power spectrum exhibits both a broad-band background and multiple peaks (not shown). As a consequence, synchronization behavior, when present, is essentially different from what we have seen in the phase-coherent regime of the previous subsection. The presence of multiple unstable periodic orbits (UPOs), with different period lengths, requires a much stronger coupling for synchronization to occur: it is only upon zero-crossing of one positive Lyapunov exponent that two or more oscillators become phase-synchronized in the funnel regime [9].

As in the phase-coherent case, we start by analyzing uncoupled subsystems and evaluate whether M-SSA is still able to distinguish between them. The more complex behavior of each oscillator leads to a more ambigu-
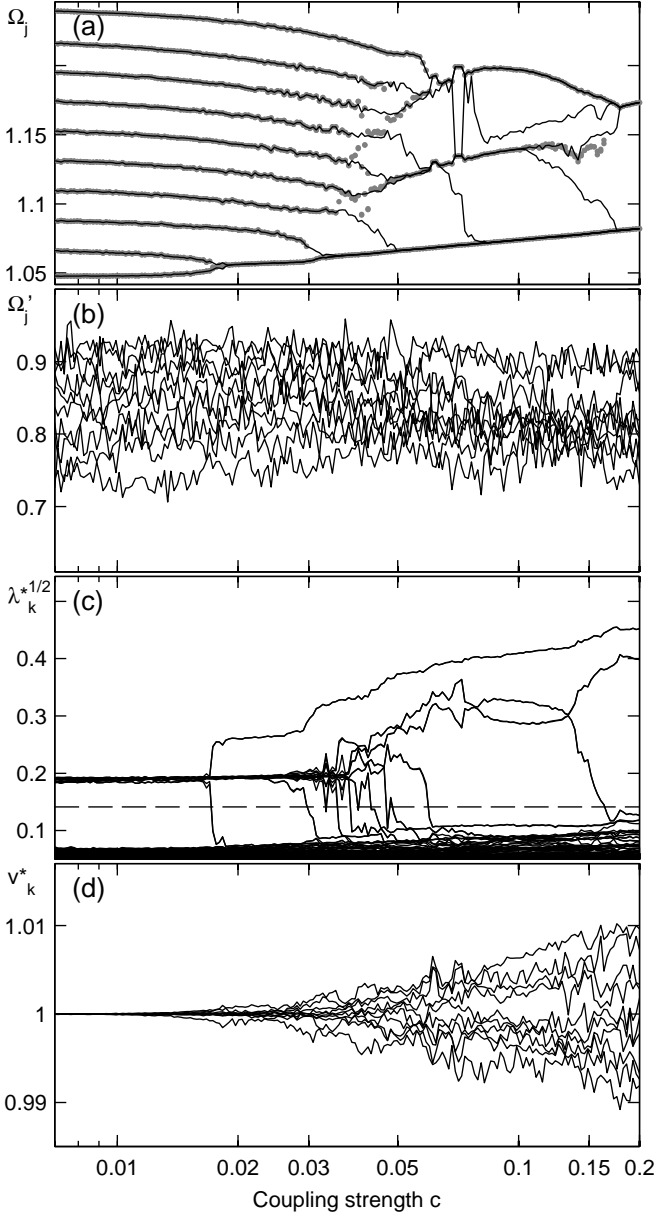
Figure 8. Same analysis as in Fig. 5 but the output of the oscillator chain being analyzed is contaminated by Gaussian noise of the same variance as the signal. (a) Estimated frequencies from rotated PCs (gray dots) and the observed frequencies Ω_j from the noiseless case (solid lines); (b) observed frequencies Ω_j' of the noise-perturbed case; (c) modified variances $\lambda_k^*, k \leq 20$, along with the unchanged eigenvalues $\lambda_k, k \geq 21$; and (d) modified eigenvalues v_k^* of the phase coupling matrix.
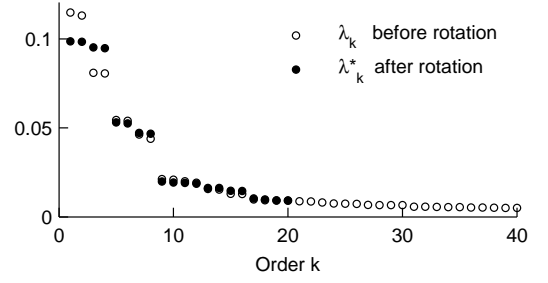

Figure 9. Eigenvalue spectrum for two uncoupled and detuned Rössler oscillators in the funnel regime ($\alpha = 0.28$): λ_k from Eq. (1), and λ_k^* from Eq. (12) after rotation of the first $S = 20$ eigenvectors. Window width $M = 30$.
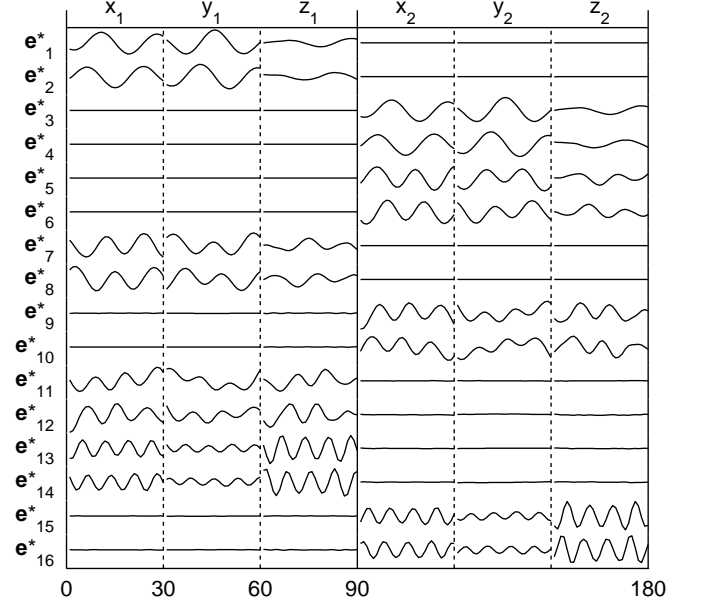

Figure 10. Rotated eigenvectors $\mathbf{e}_k^*$ associated with the 16 largest eigenvalues λ_k^* in Fig. 9.

ous eigenvalue spectrum in Fig. 9 than in Fig. 1: we observe quite a few groupings of eigenvalues λ_k, rather than two well-separated ones, and a rather slowly decaying tail. The corresponding eigenvectors (not shown) include components associated with both oscillators.

After varimax rotation, we observe two distinct groups of λ_k^*'s, namely 1–4 and 5–8, each of them containing

in turn two pairs of nearly equal values. All of the rotated eigenvectors in Fig. 10 are clearly associated with one of the two oscillators, and no mixture effects occur any longer. The complex dynamical behavior leads to multiple oscillatory pairs for each of the subsystems, and it might well be the existence of two distinct near-periodicities in the funnel regime [9] — possibly associated with two separate UPOs — that gives rise to the two distinct groups in Fig. 9. The reconstruction using just the first RC pair, for example, describes an oscillation similar to the one in the phase-coherent regime; compare Figs. 4(a) and (b).

UPOs are road posts on the way from simple to complex dynamics, leave their imprint on the system's observed time series [1], and play an important role in the synchronization process. Since the eigendecomposition of a covariance matrix gives mutually orthogonal eigenvectors, we cannot expect them to match the more com-
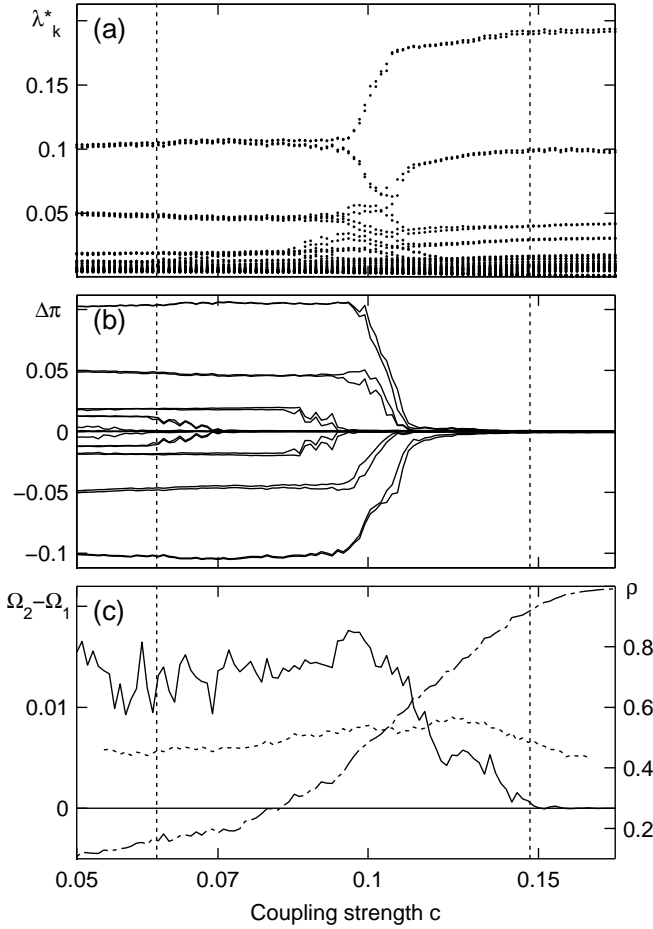
Figure 11. Synchronization of two coupled Rössler oscillators in the funnel regime. (a) Modified variances λ_k^* with $M = 30$, after rotation of the first $S = 20$ eigenvectors; and (b) difference $\Delta\pi_k$ between the oscillators' participation indices π_{dk}. (c) Difference of mean observed frequencies $\Omega_2 - \Omega_1$ (solid line) with corresponding spectral resolution (dashed line) and phase coupling strength ρ_{12} (dash-dotted line); the phase definitions follow [9]. The two vertical dashed lines indicate the transition of a zero Lyapunov exponent to negative values at $c \simeq 0.06$ and zero crossing of one positive Lyapunov exponent at $c \simeq 0.15$, respectively. All quantities are averages over 10 realizations with different initial data.

plex geometry of UPOs in the system's phase space. M-SSA is, nonetheless, able to reliably detect oscillatory modes, and provides a robust reconstruction of an approximate skeleton of the attractor from short and noisy data [2, 29, 30].

The complex synchronization process in the funnel regime is also reflected by the more complex behavior of the post-rotation variances $\{\lambda_k^*\}$ in Fig. 11(a): since the process involves the interaction of multiple UPOs, the transitions are more gradual than in the phase-coherent case, in which a single abrupt jump occurs (not shown). We obtain multiple oscillatory pairs in the eigenvalue spectrum — each with a distinct variance and frequency — and these oscillations interfere with each other in

Fig. 11(a). Furthermore, we observe that all the transitions lie between the coupling-parameter value $c \simeq 0.06$, at which a null Lyapunov exponent that is associated with motion along a limit cycle becomes negative, and the value $c \simeq 0.15$, at which one of the two positive Lyapunov exponents associated with the chaotic behavior of each Rössler oscillator falls below zero (vertical dashed lines in Fig. 11). In particular, there appear to be no transitions in λ_k^* that could be linked to the onset of phase synchronization in Fig. 11(c).

To gain greater insight into the complex interplay of distinct spectral peaks and separate subsystems, we further analyze the ability of each oscillatory mode to distinguish between the two subsystems. This is done here by computing the difference $\Delta\pi_k = \sum_{d=1,2,3} \pi_{dk} - \sum_{d=4,5,6} \pi_{dk}$ between the participation indices associated with the variables of the two oscillators: this difference is maximally positive when $\mathbf{e}_k^*$ is completely associated with the first subsystem, maximally negative for the second one, and zero if no distinction is possible.

As the coupling strength c increases, we observe in Fig. 11(b) a cascade of vanishing differences in the participation indices, with the weaker oscillatory modes getting synchronized first. In fact, M-SSA enhanced by varimax rotation indicates a complete set of synchronized oscillatory modes at $c \simeq 0.11$, well before phase synchronization occurs at $c \simeq 0.15$.

In this interval $0.11 \lesssim c \lesssim 0.15$, the two oscillators show already long epochs of phase synchronization, interrupted only by rare phase slips [9]. The difference $\Omega_2 - \Omega_1$, which is the ensemble average over 10 realizations of the system, reaches a value that is smaller than the ensemble standard deviation of either frequency (dashed line in Fig. 11(c)) at $c \simeq 0.11$. This standard deviation is induced by the effective noise due to lack of phase coherence [31, 32] and it equals the spectral resolution; as a consequence, M-SSA indicates already phase synchronization when the frequency difference falls below the spectral resolution.

This effective noise, which limits the resolution of M-SSA and that of other spectral methods, becomes quite significant in the funnel regime under study, since phase diffusion in this regime is several orders of magnitude larger than in the phase-coherent one [9]. By increasing the coupling strength further, it is possible to bring both oscillators even closer in frequency, thus reducing chaotic behavior even more and causing the associated zero-crossing of a positive Lyapunov exponent.

As in the previous subsection, it is worth noting that the M-SSA results show the same robustness against observational white noise, and Figs. 11(a-b) are practically unaffected when adding noise of the same variance as the signal (not shown). Such a high noise level, however, would impede a direct application of the phase-by-curvature definition [9] in Fig. 11(c) and require further pre-filtering.

IV. CONCLUDING REMARKS

In the present paper, we have demonstrated that multivariate singular spectrum analysis (M-SSA) provides an elegant way to obtain sharp and robust results in phase synchronization analysis. This method does not rely on a priori information about a proper phase definition, and it thus provides an entirely objective approach to the identification of oscillatory modes and of their interactions in coupled systems.

We have shown that, in the classical case of phase-and-frequency locking of spiral chaotic systems, M-SSA provides reliable and consistent information about the synchronization mechanism. To achieve the full potential of M-SSA in this respect, we have introduced a modified varimax rotation of the M-SSA eigenvectors, and shown that this simple but effective modification allows a correct identification of clusters of synchronized oscillators. For chains of coupled oscillators, moreover, M-SSA is much more robust against observational noise than common methods of phase synchronization analysis that are based on a geometric phase definition. In addition, M-SSA goes beyond pure cluster identification and allows the reconstruction of shared dynamical behavior in terms of well-defined oscillatory modes, even when the signal is getting swamped by observational white noise.

Finally, we have analyzed the funnel regime of Rössler oscillators in which phase-coherent behavior is absent, and thus no direct phase definition is possible. In this regime, the system passes through several cycles of different period length — associated with multiple unstable periodic orbits (UPOs) — and the power spectrum has a broad-band component. As a consequence, M-SSA identifies multiple oscillatory modes for each of the oscillators. It turns out that these oscillatory modes get successively synchronized as the coupling strength increases, starting from the modes with the smallest to those with the largest variance. Despite the limited explanatory power of orthogonal eigenvectors, this behavior appears to be linked to the synchronization of multiple UPOs. We have shown, furthermore, that strongly diffusive phase dynamics — which is known to reduce spectral resolution — also limits the detection of phase synchronization, and that even M-SSA cannot overcome this fundamental limitation, which arises from the physics of the situation.

In the present work, we have made the rather restrictive assumption of system contamination by white noise only. In more realistic situations, however, the noise — whether extrinsic or intrinsic — may exhibit frequency-dependent behavior, i.e. be "colored" rather than white noise, and more rigorous statistical tests for the identification of significant oscillatory modes might be required [1, 28].

Appendix A: Modified varimax rotation

In order to find a rotation matrix $\mathbf{T}$ that maximizes the varimax criterion V_1 in Eq. (6), Kaiser [23] proposed the successive pairwise rotation of eigenvectors. In this approach, all possible pairs that can be formed with the first S eigenvectors are successively rotated until a certain convergence limit in V_1 is reached. For completeness, we summarize here briefly the standard algorithm for the case $M = 1$. If not otherwise specified, the summation is over $d = 1, \ldots, D$.

Given any two eigenvectors $\mathbf{e}_k$ and $\mathbf{e}_l$, their planar rotation is given by

$$e_{dk}^* = \ \ e_{dk} \cos\phi + e_{dl} \sin\phi \,, \tag{A1}$$
$$e_{dl}^* = -\, e_{dk} \sin\phi + e_{dl} \cos\phi \,;$$

hence

$$\mathrm{d}e_{dk}^*/\mathrm{d}\phi = e_{dl}^* \,, \quad \mathrm{d}e_{dl}^*/\mathrm{d}\phi = -e_{dk}^* \,. \tag{A2}$$

The rotation angle ϕ is chosen so as to maximize the pair's V_1-value,

$$D \sum e_{dk}^{*\,4} - \left(\sum e_{dk}^{*\,2}\right)^2 + D \sum e_{dl}^{*\,4} - \left(\sum e_{dl}^{*\,2}\right)^2 , \tag{A3}$$

according to Eq. (6). Differentiating (A3) with respect to ϕ and using (A2) gives the extremal condition

$$D \sum e_{dk}^* e_{dl}^* (e_{dk}^{*\,2} - e_{dl}^{*\,2}) - \sum e_{dk}^* e_{dl}^* \cdot \sum (e_{dk}^{*\,2} - e_{dl}^{*\,2}) = 0. \tag{A4}$$

Substitution of e_{dk}^* and e_{dl}^* according to (A1) yields an explicit equation for ϕ in terms of e_{dk} and e_{dl} [23].

The derivation requires an extensive amount of algebraic manipulation, and it is only sketched in the appendix of [23]. The full derivation is not necessary, however, in order to understand the implications of the modified varimax criterion (8) we propose.

We start with the orthogonal rotation of two M-SSA eigenvectors,

$$e_{dk}^*(m) = \ \ e_{dk}(m) \cos\phi + e_{dl}(m) \sin\phi \,, \tag{A5}$$
$$e_{dl}^*(m) = -\, e_{dk}(m) \sin\phi + e_{dl}(m) \cos\phi \,,$$

which yields

$$\mathrm{d}e^*_{dk}(m)/\mathrm{d}\phi = e^*_{dl}(m), \quad \mathrm{d}e^*_{dl}(m)/\mathrm{d}\phi = -e^*_{dk}(m)\,, \quad \text{(A6)}$$

and hence

$$
\begin{aligned}
\frac{\mathrm{d}\bar{e}^*_{dk}}{\mathrm{d}\phi} &= \frac{\sum_{m=1}^{M} e^*_{dk}(m)e^*_{dl}(m)}{\bar{e}^*_{dk}}\,, \\
\frac{\mathrm{d}\bar{e}^*_{dl}}{\mathrm{d}\phi} &= -\frac{\sum_{m=1}^{M} e^*_{dk}(m)e^*_{dl}(m)}{\bar{e}^*_{dl}}\,.
\end{aligned}
\qquad \text{(A7)}
$$

According to (8), we choose the rotation angle ϕ so as to maximize

$$D \sum \bar{e}^{*}_{dk}{}^{4} - \left(\sum \bar{e}^{*}_{dk}{}^{2}\right)^2 + D \sum \bar{e}^{*}_{dl}{}^{4} - \left(\sum \bar{e}^{*}_{dl}{}^{2}\right)^2. \quad \text{(A8)}$$

As for Eqs. (A3) and (A4), we differentiate (A8) with respect to ϕ, using (A7), and obtain the extremal condition

$$
\begin{aligned}
0 = {}& D \sum \sum_m e^*_{dk}(m)e^*_{dl}(m)(\bar{e}^{*}_{dk}{}^{2} - \bar{e}^{*}_{dl}{}^{2}) \\
& - \sum \sum_m e^*_{dk}(m)e^*_{dl}(m) \cdot \sum (\bar{e}^{*}_{dk}{}^{2} - \bar{e}^{*}_{dl}{}^{2})\,.
\end{aligned}
\qquad \text{(A9)}
$$

Equation (A9) only differs from (A4) by an additional summation over m: the terms $e^*_{dk}e^*_{dl}$ and $e^{*}_{dk}{}^{2} - e^{*}_{dl}{}^{2}$ in (A4) are simply replaced by $\sum_m e^*_{dk}(m)e^*_{dl}(m)$ and $\bar{e}^{*}_{dk}{}^{2} - \bar{e}^{*}_{dl}{}^{2} \equiv \sum_m (e^{*}_{dk}{}^{2}(m) - e^{*}_{dl}{}^{2}(m))$, respectively. It suffices, therefore, to understand the implications of this replacement. According to (A5), substitution of $e^*_{dk}(m)$ and $e^*_{dl}(m)$ yields

$$
\begin{aligned}
\sum_m e^*_{dk}(m)e^*_{dl}(m) &= -f(\phi)\sum_m e^2_{dk}(m) + f(\phi)\sum_m e^2_{dl}(m) + g(\phi)\sum_m e_{dk}(m)e_{dl}(m)\,, \\
\bar{e}^{*}_{dk}{}^{2} - \bar{e}^{*}_{dl}{}^{2} &= g(\phi)\sum_m e^2_{dk}(m) - g(\phi)\sum_m e^2_{dl}(m) + 4f(\phi)\sum_m e_{dk}(m)e_{dl}(m)\,,
\end{aligned}
\qquad \text{(A10)}
$$

with $f(\phi) = \sin\phi\cos\phi$ and $g(\phi) = \cos^2\phi - \sin^2\phi$. Hence, we simply have to replace $e^2_{d,\cdot}$ by $\sum_m e^2_{d,\cdot}(m)$, and $e_{dk}e_{dl}$ by $\sum_m e_{dk}(m)e_{dl}(m)$ in the equation for the rotation angle ϕ of Ref. [23].

[1] M. Ghil, M. R. Allen, M. D. Dettinger, K. Ide, D. Kondrashov, M. E. Mann, A. W. Robertson, A. Saunders, Y. Tian, F. Varadi, and P. Yiou, Rev. Geophys. **40**, 1 (2002).
[2] R. Vautard and M. Ghil, Physica D **35**, 395 (1989).
[3] M. Ghil and R. Vautard, Nature **350**, 324 (1991).
[4] D. S. Broomhead, R. Jones, and G. P. King, J. Phys. A: Math. Gen. **20**, L563 (1987).
[5] M. Paluš and I. Dvorák, Physica D **55**, 221 (1992).
[6] S. Boccaletti, J. Kurths, G. Osipov, D. L. Valladares, and C. S. Zhou, Physics Reports **366**, 1 (2002).
[7] A. Pikovsky, M. Rosenblum, and J. Kurths, *Synchronization: A Universal Concept in Nonlinear Science* (Cambridge University Press, 2003).
[8] M. Rosenblum, A. Pikovsky, and J. Kurths, Phys. Rev. Lett. **76**, 1804 (1996).
[9] G. Osipov, B. Hu, C. Zhou, M. Ivanchenko, and J. Kurths, Phys. Rev. Lett. **91**, 024101 (2003).
[10] I. Z. Kiss, Q. Lv, and J. L. Hudson, Phys. Rev. E **71**, 035201 (2005).
[11] Y. Feliks, M. Ghil, and A. W. Robertson, J. Clim. **23**, 4060 (2010).
[12] G. Osipov, A. Pikovsky, M. Rosenblum, and J. Kurths, Phys. Rev. E **55**, 2353 (1997).
[13] D. S. Broomhead and G. P. King, Physica D **20**, 217 (1986).
[14] D. S. Broomhead and G. P. King, in *Nonlinear Phenomena and Chaos*, edited by S. Sarkar (Adam Hilger, Bristol, England, 1986) pp. 113–144.
[15] R. Vautard, P. Yiou, and M. Ghil, Physica D **58**, 95 (1992).
[16] A. V. Oppenheim and R. W. Schafer, *Discrete-Time Signal Processing*, 3rd ed. (Prentice Hall Press, Upper Saddle River, NJ, USA, 2009).
[17] G. Plaut and R. Vautard, J. Atmos. Sci. **51**, 210 (1994).
[18] M. Müller, G. Baier, A. Galka, U. Stephani, and H. Muhle, Phys. Rev. E **71**, 046116 (2005).
[19] C. Allefeld, M. Müller, and J. Kurths, Int. J. Bifurcat. Chaos **17**, 3493 (2007).
[20] G. R. North, T. L. Bell, R. F. Cahalan, and F. J. Moeng, Mon. Wea. Rev. **110**, 699 (1982).
[21] S. Bialonski and K. Lehnertz, Phys. Rev. E **74**, 051909 (2006).
[22] M. Vejmelka and M. Paluš, Chaos **20**, 033103 (2010).
[23] H. Kaiser, Psychometrika **23**, 187 (1958).
[24] I. T. Jolliffe, *Principal Component Analysis*, 2nd ed., Springer Series in Statistics (Springer New York, 2002).
[25] M. B. Richman, Int. J. Climatol. **6**, 293 (1986).
[26] R. B. Cattell, Mult. Behav. Res. **1**, 245 (1966).
[27] E. A. O'Lenic and R. E. Livezey, Mon. Wea. Rev. **116**, 1682 (1988).
[28] M. R. Allen and L. A. Smith, J. Climate **9**, 3373 (1996).

[29] M. Kimoto and M. Ghil, J. Atmos. Sci. **50**, 2645 (1993).

[30] M. Ghil and P. Yiou, in *Decadal Climate Variability: Dynamics and Predictability*, edited by D. Anderson and J. Willebrand (Springer-Verlag, Berlin/Heidelberg, 1996) pp. 446–482.

[31] A. Pikovsky, M. Rosenblum, G. Osipov, and J. Kurths, Physica D **104**, 219 (1997).

[32] J. D. Farmer, Phys. Rev. Lett. **47**, 179 (1981).